ORNL/CP-98361

POLYCRYSTAL SIMULATIONS OF TEXTURE EVOLUTION DURING DEFORMATION PROCESSING

G. Sarma, B. Radhakrishnan, and T. Zacharia

Oak Ridge National Laboratory
P.O. Box 2008, MS-6140
Oak Ridge, TN 37831-6140, USA

Abstract

Some recent research on the hot deformation of aluminum alloys has indicated that at elevated temperatures, slip occurs on $\{110\}\langle 110\rangle$ systems in addition to the usual $\{111\}\langle 110\rangle$ systems active at lower temperatures. The effect of these additional slip systems on the texture evolution of aluminum single and polycrystals is studied using finite element simulations. The crystals are deformed in plane strain compression, and the constitutive response is modeled using crystal plasticity to track the reorientation of the crystals. By discretizing each crystal with a large number of elements, the non-uniform deformations due to local inhomogeneities and interactions with neighboring crystals are modeled. The resulting textures and microstructures are examined with regard to effect of including the additional systems, initial orientation of the single crystals, and stability of the cube orientation.

DISCLAIMER

Introduction

It is well known that plastic deformation in fcc metals is accommodated by slip on $\{111\}$ planes in $\langle 110\rangle$ directions. This knowledge has been utilized in the application of crystal plasticity models to study the texture development during cold working of aluminum and its alloys. It has been postulated that when aluminum is deformed at elevated temperatures, slip occurs on other planes, notably $\{100\}$, $\{110\}$ and $\{112\}$ [1,2]. Slip activity on the non-octahedral systems alters the relative strength of various texture components during deformation in plane strain compression. In particular, the $\{011\}\langle 211\rangle$ brass component is enhanced by slip on $\{112\}$ planes, and the $\{001\}\langle 100\rangle$ cube component is stabilized by slip on $\{110\}$ planes.

The objective of the work described in this paper is to investigate through numerical studies the effect of including the $\{110\}\langle 110\rangle$ slip systems on the texture development of aluminum. To this end, deformations of aluminum single and polycrystals in plane strain compression have been modeled using the finite element method. By discretizing the individual crystals with a large number of elements, the approach enables modeling the inhomogeneous deformations of individual grains in the microstructure. The constitutive response of the elements is modeled using crystal plasticity to track the changes in orientation, and hence the texture evolution. Such mesoscale modeling of polycrystals is being increasingly used to gain insights into the local variations in deformation and texture development due to interactions among different grains in the microstructure [3–5].

Since the cube orientation is an important component of the textures obtained after hot rolling and subsequent annealing of aluminum alloys, the focus of this study has been to examine the stability of this component. Experiments on cube oriented single crystals deformed in plane strain compression have shown that this orientation is stable at high temperatures, but rotates away about the transverse direction (TD) and/or normal direction (ND) at low temperatures [6,7]. In order to examine the stability of the cube orientation, deformations of single crystals with starting orientations at and near cube were simulated, without and with the $\{110\}\langle 110\rangle$ slip systems. The effect of including slip on $\{110\}$ planes was also examined in polycrystalline aggregates, both with and without an initial cube oriented grain. In this case, the cube grain is influenced by the constraints from neighboring grains. The results of the analyses indicate that inclusion of $\{110\}$ planes tends to stabilize the cube orientation, whereas excluding them causes cube oriented regions to rotate away.

Finite Element Formulation

The finite element formulation used for the present study follows the hybrid formulation described by Beaudoin et al. [8]. It is assumed that elastic deformations are negligibly small, and that deformation occurs by slip dominated plastic flow of the material. Due to the limited modes of deformation available through slip, the crystal must rotate to accommodate arbitrary deformations. The resulting texture development is modeled using a constitutive law based on crystal plasticity.

A viscoplastic constitutive law relates the rate of shearing $\dot{\gamma}^{(\alpha)}$ to the resolved shear stress $\tau^{(\alpha)}$ on each slip system (α)

$$\dot{\gamma}^{(\alpha)} = \dot{\gamma}_0 \left| \frac{\tau^{(\alpha)}}{\hat{\tau}} \right|^{\frac{1}{m}} \operatorname{sign}(\tau^{(\alpha)}), \tag{1}$$

where m is the rate sensitivity parameter, and $\dot{\gamma}_0$ is a reference rate of shearing. $\hat{\tau}$ is a hardness parameter which represents resistance to plastic deformation due to interactions among dislocations. The resolved shear stress is the component of the traction along the slip direction, and is obtained from the crystal deviatoric Cauchy stress $\boldsymbol{\sigma}'_c$ using the Schmid tensor (dyadic product of the slip direction $\boldsymbol{s}^{(\alpha)}$ and the slip plane normal $\boldsymbol{n}^{(\alpha)}$ vectors),

$$\tau^{(\alpha)} = \boldsymbol{\sigma}'_c \boldsymbol{n}^{(\alpha)} \cdot \boldsymbol{s}^{(\alpha)} = \boldsymbol{\sigma}'_c \cdot \boldsymbol{T}^{(\alpha)} = \boldsymbol{\sigma}'_c \cdot \boldsymbol{P}^{(\alpha)}. \tag{2}$$

In the above expression, $\boldsymbol{P}^{(\alpha)}$ is the symmetric portion of the Schmid tensor $\boldsymbol{T}^{(\alpha)}$, and is used to express the crystal rate of deformation $\boldsymbol{D}_c$ as a linear combination of the slip system shearing rates,

$$\boldsymbol{D}_c = \sum_{\alpha} \dot{\gamma}^{(\alpha)} \boldsymbol{P}^{(\alpha)}. \tag{3}$$

The crystal rate of deformation is the symmetric part of the crystal velocity gradient, and prescribes the rate of shearing of slip planes. The skew-symmetric part of the crystal velocity gradient $\boldsymbol{W}_c$ controls the rotation of the crystal, and contains contributions from both the spin associated with the plastic flow, and the rigid rotation $\boldsymbol{R}^*$ of the crystal lattice necessary to maintain compatibility with neighboring crystals,

$$\boldsymbol{W}_c = \dot{\boldsymbol{R}}^* \boldsymbol{R}^{*T} + \sum_{\alpha} \dot{\gamma}^{(\alpha)} \boldsymbol{Q}^{(\alpha)}, \tag{4}$$

where $\boldsymbol{Q}^{(\alpha)}$ is the skew-symmetric part of the Schmid tensor $\boldsymbol{T}^{(\alpha)}$. Rewriting equation (4) results in the crystal reorientation rate $\dot{\boldsymbol{R}}^*$, given by the difference between the crystal spin and the plastic spin due to slip,

$$\dot{\boldsymbol{R}}^* = \left(\boldsymbol{W}_c - \sum_{\alpha} \dot{\gamma}^{(\alpha)} \boldsymbol{Q}^{(\alpha)} \right) \boldsymbol{R}^*. \tag{5}$$

Eliminating $\dot{\gamma}^{(\alpha)}$ between equations (1) and (3), and substituting equation (2) for $\tau^{(\alpha)}$ leads to an expression for the crystal deformation rate in terms of the deviatoric stress,

$$\boldsymbol{D}_c = \left[\sum_{\alpha} \frac{\dot{\gamma}_0}{\hat{\tau}} \left| \frac{\tau^{(\alpha)}}{\hat{\tau}} \right|^{\frac{1}{m}-1} \boldsymbol{P}^{(\alpha)} \otimes \boldsymbol{P}^{(\alpha)} \right] \boldsymbol{\sigma}'_c = \mathcal{S}_c \boldsymbol{\sigma}'_c, \tag{6}$$

where $\mathcal{S}_c$ is the fourth-order crystal "compliance" tensor. The rate dependence of equation (1) permits inversion of equation (6), and expression of the crystal deviatoric stress under a given deformation rate as

$$\boldsymbol{\sigma}'_c = \mathcal{S}_c^{-1} \boldsymbol{D}_c. \tag{7}$$

The non-linear nature of the crystal constitutive equation (7) requires an iterative method to compute the deviatoric stress for a given rate of deformation. The anisotropic response due to the crystal orientation is reflected in the crystal compliance.

The plastic deformation of the material is modeled in incremental fashion, by solving the boundary value problem for material motion at each strain increment. Balance laws for equilibrium and mass conservation are applied in conjunction with the constitutive assumptions discussed above. Following the approach of Beaudoin et al. [8], a hybrid finite element formulation is employed for this purpose. Instead of developing the equilibrium statement from balance of momentum at the global level, here it is written as a balance of tractions at the inter-element boundaries. Weighted residuals are formed on the equilibrium statement and the constitutive relation. A third residual on the conservation of

mass (which for the case of incompressible plastic deformation reduces to a divergence-free velocity field) completes the formulation. Interpolation functions are introduced for the nodal velocities, element stress components and the pressure. A proper choice of the shape functions for the stress permits elimination of the stress degrees of freedom at the element level. The result is a system of equations for the discretized velocity field, which is solved assuming fixed material state and geometry.

Upon obtaining a converged velocity solution, the material state and geometry are updated. The material is characterized by the orientation of the crystal and the hardness parameter. The reorientation rate given by equation (5) is used to update the orientation, while the hardness is evolved using a modified Voce type law,

$$\dot{\hat{\tau}} = H_0 \left(\frac{\hat{\tau}_s - \hat{\tau}}{\hat{\tau}_s - \hat{\tau}_i} \right) \dot{\gamma}^*, \tag{8}$$

where hardening rate H_0 and initial hardness $\hat{\tau}_i$ are material parameters. $\dot{\gamma}^*$ is a measure of the net shearing rate on all the slip systems,

$$\dot{\gamma}^* = \sum_{\alpha} \left| \dot{\gamma}^{(\alpha)} \right|. \tag{9}$$

The saturation hardness $\hat{\tau}_s$ based on the current slip system state is given by

$$\hat{\tau}_s = \hat{\tau}_{s_0} \left(\frac{\dot{\gamma}^*}{\dot{\gamma}_s} \right)^{m'}, \tag{10}$$

where $\hat{\tau}_{s_0}$, $\dot{\gamma}_s$ and m' are material parameters.

Development of the material response entails solution of the non-linear crystal constitutive relation for each element, and must be performed during each iteration for the velocity field at a given strain increment. In this respect, the methodology described above proves to be computationally demanding. Use of the hybrid approach leads to introduction of additional degrees of freedom for the crystal stresses, thereby adding to the computational burden associated with the stiffness calculations. The advantage of using this approach is the smoothness in the stress field, due to the enforcement of traction balance at the element interfaces in an approximate sense [8]. In the finite element context, the numerical integration required for computing the stiffness matrix can be performed concurrently for all elements. The choice of piecewise discontinuous interpolation functions for the stress is a key feature of the formulation, which enables computation of the stiffness matrices in concurrent fashion for all elements. In turn, this feature permits exploitation of parallel computing technologies in order to greatly improve the feasibility of treating large three-dimensional discretizations.

While the stiffness computations are relatively straightforward to implement in a parallel environment, the solution of the resulting system of equations poses a greater challenge. Since direct solvers are difficult to optimize on a parallel machine, it is advantageous to use an iterative procedure, such as the conjugate gradient method. In this context, enforcing the incompressibility constraint requires special attention, since it degrades the numerical condition of the resulting system of equations. In the current formulation, incompressibility is enforced using a modified consistent penalty approach, which seeks to decouple the solution for the pressure field from the conjugate gradient method [9]. Details of the parallel implementation of the formulation on the Intel PARAGON are available elsewhere [10].

Application to Single Crystals

The formulation described above has been applied to simulate the deformation of single crystals of aluminum with different orientations. For each simulation, the crystal was discretized with 4096 elements arranged in the form of a cube with 16 elements along each side. The inner 1000 elements were used for examining the texture development. At the start of the simulations, all 4096 elements were assigned the same orientation. Boundary conditions corresponding to plane strain compression were applied to the mesh. The faces normal to $-$X and $-$Z were constrained to have no normal velocity components, as were the faces along the Y-axis (TD). The nodes on the face normal to Z (ND) had prescribed velocities such that a unit compressive deformation rate was maintained. Deformation was modeled using compressive strain increments of 1%. Material parameters used for the simulations, based on mechanical test data for aluminum [11], are listed in Table I. The critical resolved shear stress was assumed to be the same for all slip systems (for both $\{111\}$ and $\{110\}$ planes).

Table I. Material parameters for the deformation simulations.

m	$\dot{\gamma}_0$	H_0	$\hat{\tau}_i$	τ_{s0}	$\dot{\gamma}_s$	m'
0.05	1.0 s^{-1}	58.41 MPa	27.17 MPa	61.80 MPa	5.0×10^{10} s^{-1}	0.005

The deformation of a crystal with cube orientation (001)[100] was modeled first, using both 12 ($\{111\}\langle110\rangle$) and 18 ($\{111\}\langle110\rangle$ and $\{110\}\langle110\rangle$) slip systems. The results showed that for both cases, the orientation is stable for very large strains, and is able to deform in plane strain compression with no reorientation. The initial and deformed meshes are shown in Figure 1 for deformation with 12 slip systems, indicating the uniform deformation of the cube oriented crystal. Experiments on plane strain compression of cube oriented single crystals have shown that it is not stable at low temperatures but is at high temperatures [8]. For the crystal at exact cube, examination of the slip system activity reveals that the deformation is accommodated by equal slip on the complementary systems $(11\bar{1})[101]$, $(1\bar{1}\bar{1})[101]$, $(1\bar{1}1)[10\bar{1}]$ and $(111)[10\bar{1}]$, so that the crystal continues to deform with no rotation. Deviations from the mathematically exact cube orientation can be expected to lead to variations in the slip system activity, and hence to non-uniform deformation.

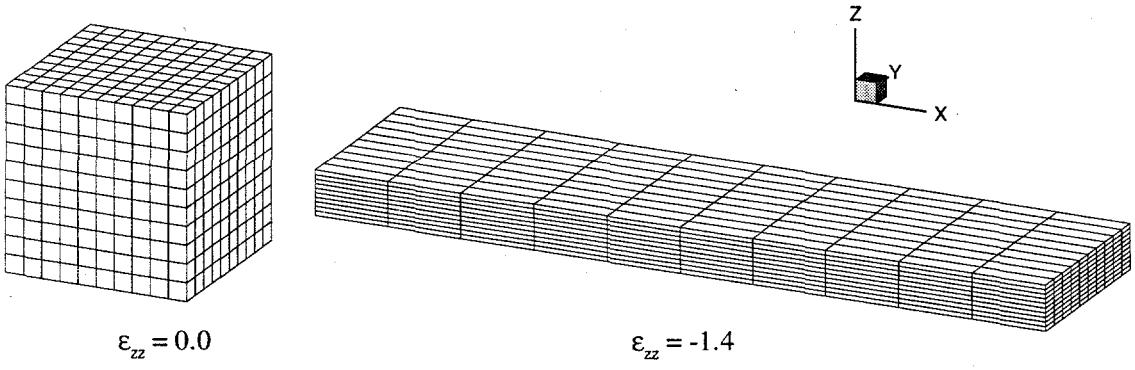

Figure 1: Initial and deformed meshes for inner 1000 elements from plane strain compression of cube oriented crystal using 12 slip systems.

The deformation of a crystal misoriented by a small amount from the cube orientation was modeled using 12 and 18 slip systems. The initial orientation of the crystal was taken

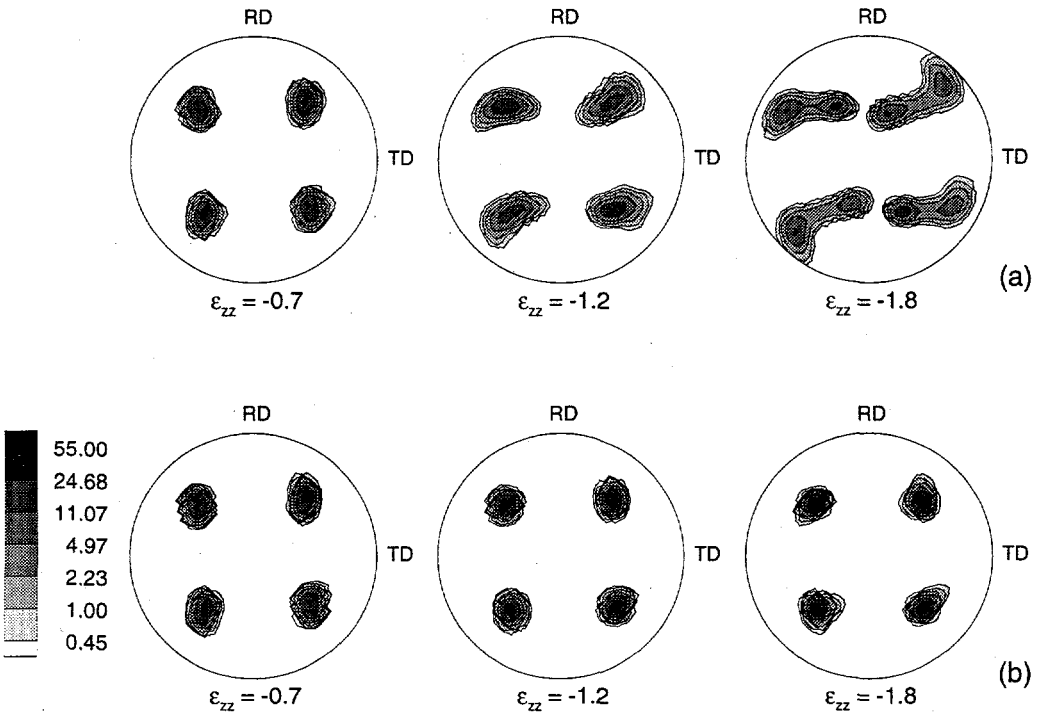

Figure 2: $\langle 111 \rangle$ pole figures in equal area projection showing texture evolution of a crystal slightly misoriented from cube, deformed in plane strain compression using (a) 12 slip systems, and (b) 18 slip systems.

to be (0°, 5°, 5°) in terms of Euler angles using Kocks convention[1] [12]. The texture evolution computed using the orientations of the inner 1000 elements is shown in Figure 2 for the two cases. The $\langle 111 \rangle$ pole figures in equal area projection were computed using routines from the popLA [13] software package. After 50% reduction ($\varepsilon_{zz} = -0.7$), there is not a noticeable difference between the two textures. With further deformation, the crystal deforming with 12 slip systems begins to show deviation from its initial orientation. After about 83% reduction ($\varepsilon_{zz} = -1.8$), the texture consists of two main peaks, but shows appreciable spread about the peaks. The crystal deformed using 18 slip systems shows some inhomogeneity, but in this case the initial misorientation from cube gradually disappears, with all the elements rotating towards cube orientation. The initial orientation represented by its natural invariants (axis-angle pair) [14] leads to a misorientation of 7° from cube. After deformation to $\varepsilon_{zz} = -1.8$, more than 85% of the elements are misoriented by less than 5° from cube for the 18 slip system case, whereas with 12 slip systems that number is less than 6%.

The deformed meshes for the crystal misoriented from cube after 70% reduction are shown in Figure 3 for both 12 and 18 slip systems. Both cases show significant Z-X shear deformation in the same direction, and smaller degree of X-Y shear in opposite directions. Deformation with 12 slip systems also leads to some Y-Z shear, which is not as pronounced with 18 slip systems. The deformation is far more uniform with 18 slip systems, leading to the sharp cube texture, whereas the greater inhomogeneity for the 12 slip system case leads to more diffuse texture. It is hence clear that the addition of the $\{110\}\langle 110 \rangle$ slip systems tends to stabilize the cube orientation during plane strain compression.

[1] (0°, 5°, 85°) in terms of Euler angles using Bunge notation

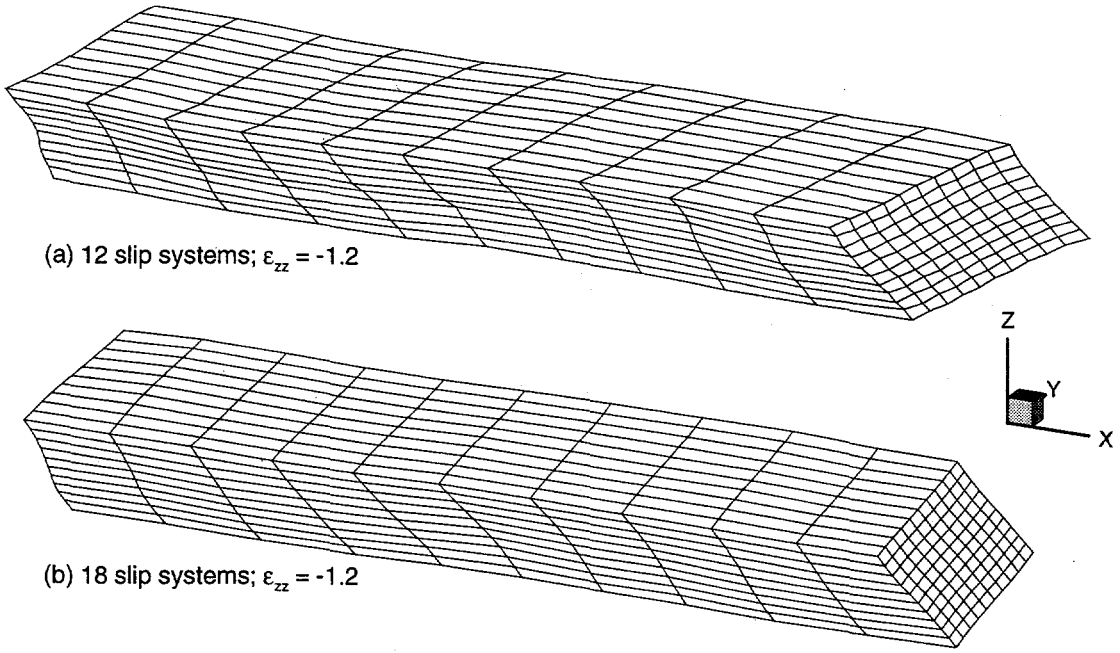

Figure 3: Deformed meshes for inner 1000 elements from plane strain compression of a crystal slightly misoriented from cube using (a) 12 slip systems, and (b) 18 slip systems.

Application to Polycrystals

In the previous section, the deformations of single crystals at and near cube orientation were considered with and without $\{110\}\langle 110\rangle$ slip systems. The crystals were not influenced by the presence of neighboring grains, as would be the case in a microstructure. In this section we consider the deformation of an aggregate of grains, each of which is discretized with finite elements to model its non-uniform deformation in the presence of constraints from the surrounding grains. The simulation procedure was applied to a microstructure consisting of 53 grains, discretized using a total of 27,000 elements arranged in a 15×30×60 mesh. The initial mesh and microstructure are shown in Figure 4(a), where the different shades of gray in the microstructure indicate different grains. The initial orientations of the grains were chosen from a random sampling of Euler space, but since each grain is weighted by the number of elements used to discretize it, the initial texture is not random. The microstructure was deformed in plane strain compression to a compressive strain of $\varepsilon_{zz} = 0.7$ (50% reduction in height), using 12 and 18 slip systems. The deformed mesh after deformation using 12 slip systems is shown in Figure 4(b), and depicts the inhomogeneous deformations of the grains. The final texture predicted using 12 slip systems is shown in Figure 5 in the form of pole figures. The pole figures were constructed from the 27,000 final orientations after applying cubic crystal symmetry and orthotropic sample symmetry. The pole figures show features typical of rolling textures, and the influence of the initial texture leads to a strong $\{123\}\langle 634\rangle$ S component and a weaker $\{112\}\langle 111\rangle$ copper component [15]. The same microstructure was also deformed using 18 slip systems, and the resulting pole figures look very similar to the those obtained using 12 slip systems. While the textures as a whole are very similar, there are some variations in the individual element reorientations, with the misorientation among corresponding elements exceeding 50° in some cases. For most of the grains the difference between deformation with 12 and 18 slip systems is minor, with only a small fraction of the elements comprising the grains being misoriented by more than 10°. But a few of the grains show significant misorientations for a large fraction of elements after deformation with 12 and 18 slip systems.

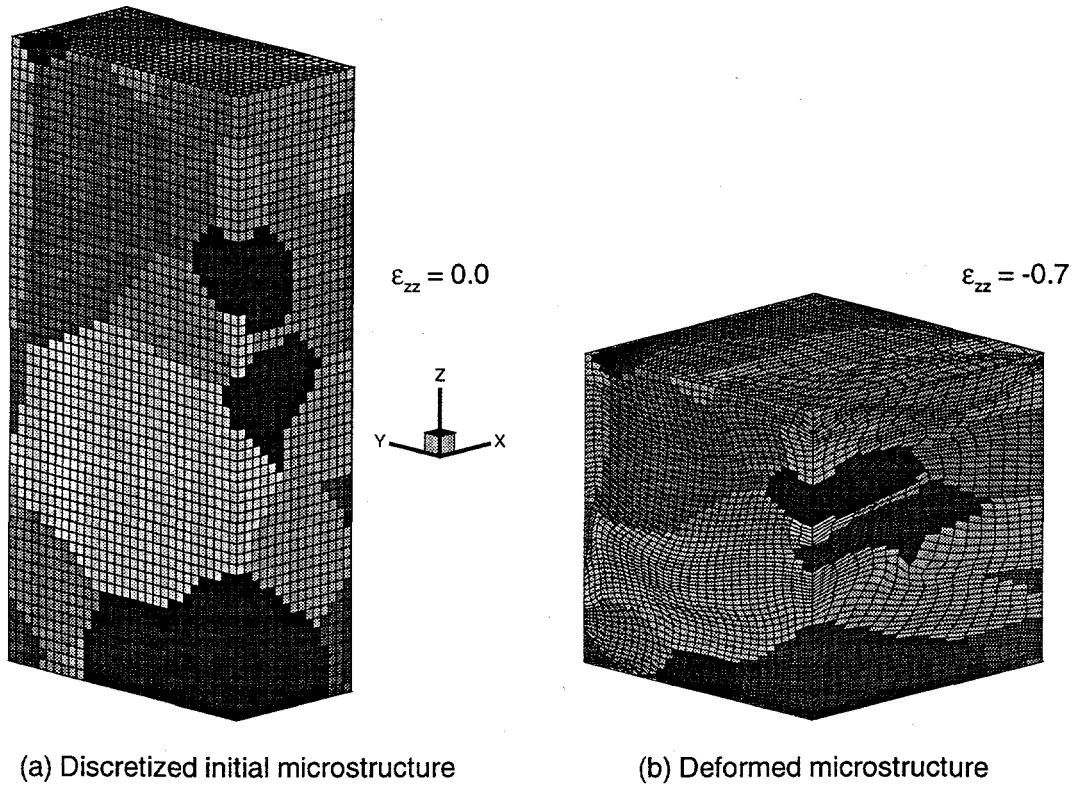

Figure 4: Initial and deformed mesh and microstructure for polycrystal simulations using 12 slip systems.

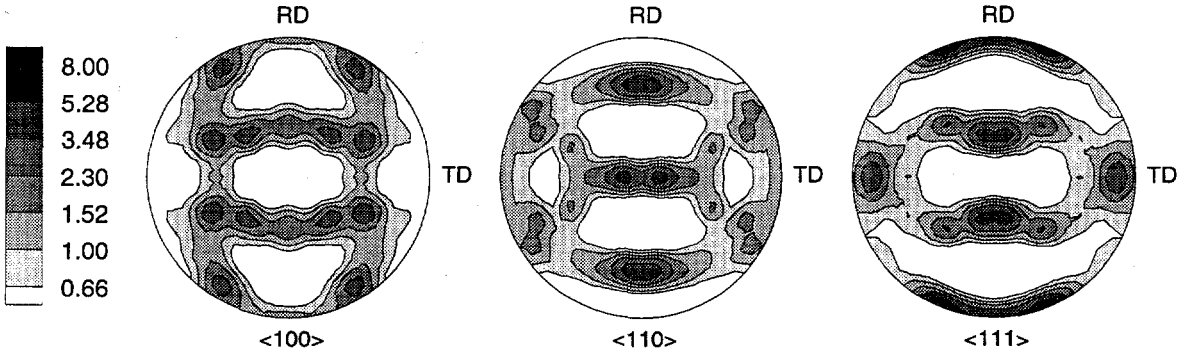

Figure 5: Pole figures in equal area projection showing the texture after deformation to $\varepsilon_{zz} = -0.7$ using 12 slip systems for the microstructure without initial cube grain.

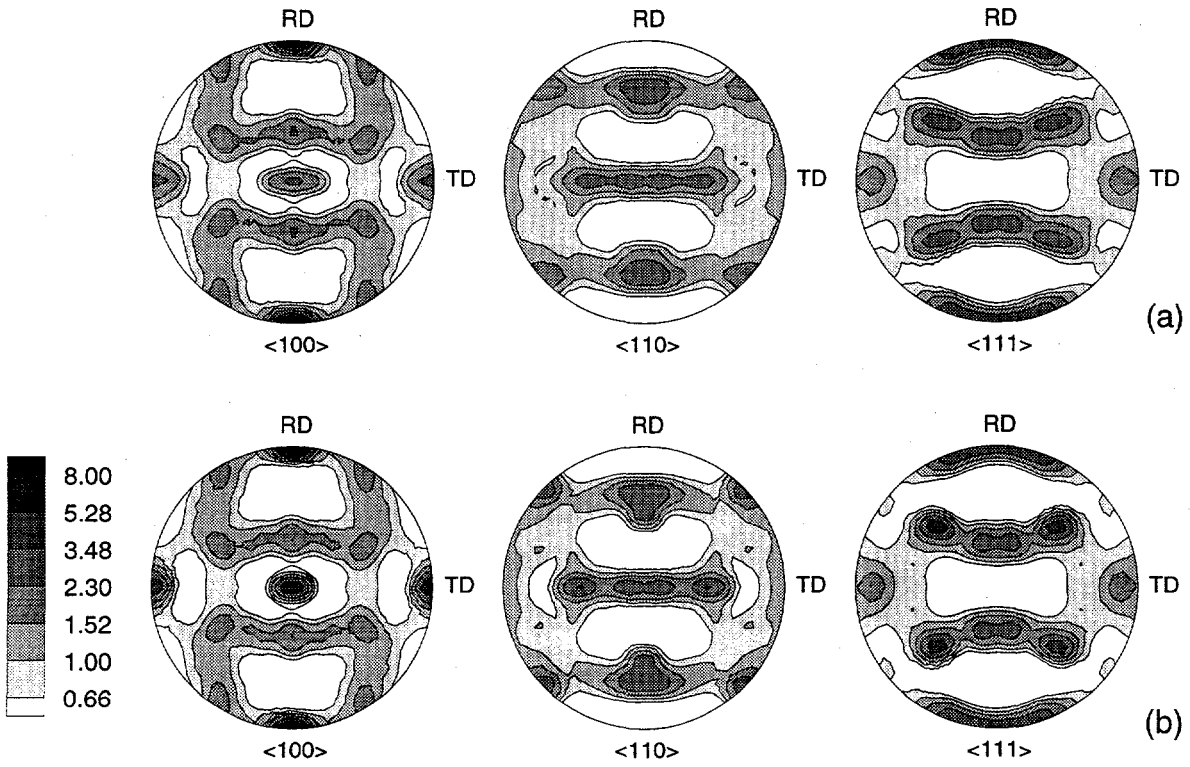

Figure 6: Pole figures in equal area projection showing the texture after deformation to $\varepsilon_{zz} = -0.7$ using (a) 12 slip systems, and (b) 18 slip systems for the microstructure with initial cube grain.

The simulations described above were repeated with the same grain structure, but this time the initial orientation of the largest grain was taken to be cube. Figures 6 shows the texture after 50% reduction for deformation with 12 and 18 slip systems. The two textures are very similar except for the peak intensity values at the cube orientation. The simulation using 18 slip systems leads to a much stronger cube component, indicating once again the stabilizing effect of slip on $\{110\}$ planes.

The influence of the slip systems on the deformation of the cube oriented grain is examined through the spread of the orientations of the elements comprising the grain after 50% reduction. The orientations were converted from Euler angles to axis-angle pairs[2], and the resulting histogram for the distribution of angles is shown in Figure 7. Since the cube orientation coincides with the reference axes, the angle of rotation also represents the deviation from cube. The histogram for 18 slip systems shows that most of the elements are misoriented from cube by less than 10°, with very few elements rotating away by more than 15°. The opposite is true for the case of 12 slip systems, with far greater number of elements misoriented by high angles. The influence of the neighboring grains in the microstructure causes the initially cube oriented grain to rotate away, but slip on $\{110\}$ planes retards the rate of rotation.

In order to study the influence of proximity to the grain boundary on the elements with initial cube orientation, they were classified as interior or boundary elements, depending on whether the adjacent elements belonged to the same or different grain in the initial microstructure. The number of adjacent elements was varied to get sets of boundary

[2]cubic crystal symmetry was used to determine the symmetrically equivalent axis and angle with the smallest angle of rotation

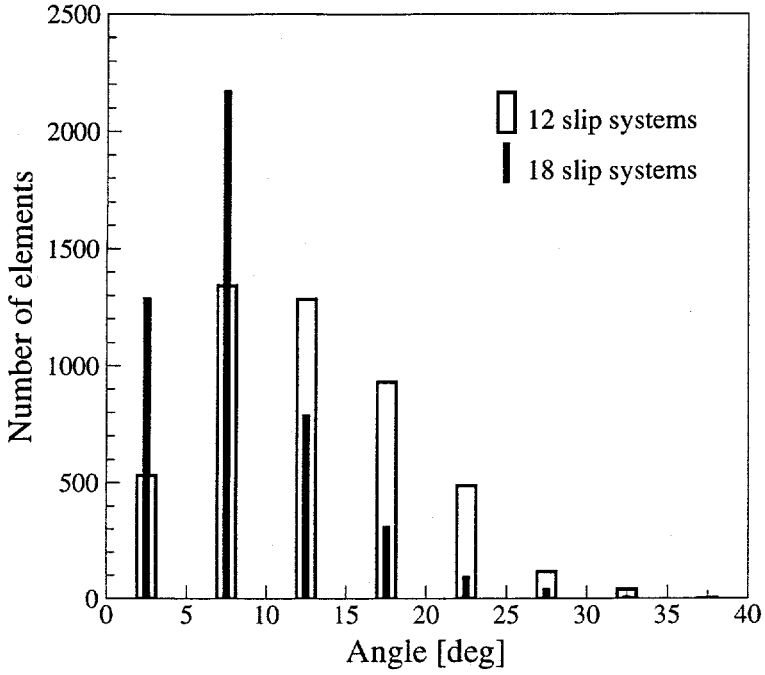

Figure 7: Histograms showing distribution of angles of rotation for the elements comprising the initially cube oriented grain.

elements of different thicknesses. Table II shows the comparison between the 18 and 12 slip system cases for different thickness values for the boundary elements. As the boundary thickness increases, the maximum angle of rotation for the interior elements decreases for both cases. But the decrease is far greater for 18 slip systems, with a maximum deviation from cube of only $\approx 18°$ when the boundary is four elements thick, compared to $\approx 27°$ for 12 slip systems. The increase in the maximum angle from the interior to the boundary indicates the effect of neighboring grains on the deformation.

Table II. Comparison of interior and boundary regions of initially cube oriented grain.

Thickness of boundary elements	Maximum θ among interior elements		Interior elements with $\theta < 10°$ (%)		Boundary elements with $\theta < 10°$ (%)	
	18 slip systems	12 slip systems	18 slip systems	12 slip systems	18 slip systems	12 slip systems
1	31.5°	34.2°	76.0	38.6	65.0	42.1
2	23.0°	30.4°	78.4	36.7	67.1	42.9
3	18.4°	28.6°	78.7	34.2	69.9	42.8
4	17.9°	27.2°	77.9	31.2	71.6	42.5

Another indication of the difference between 12 and 18 slip systems comes from examining the percent of interior and boundary elements which remain close to cube after deformation. As seen from Table II, the fraction of elements which rotate by less than 10° away from initial cube is greater for 18 slip systems for both interior and boundary elements. The fraction of interior elements with small misorientation from cube remains close to 78% with different boundary thickness values. The fraction of boundary elements with $\theta < 10°$ goes down as the boundary thickness reduces, indicating the increasing effect of neighboring grains as one gets closer to the boundary.

The boundary effect is also seen for the case of 12 slip systems, although the trend is reversed. As the boundary thickness increases, causing fewer elements to be considered as part of the interior, the fraction of interior elements with small misorientation from cube decreases. This means that as one goes towards the interior of the grain, one finds fewer grains with small misorientation from cube. Near the boundary, the effect of neighboring grains is in fact to retard the rotation away from cube, so that the fraction of boundary elements with small misorientation from cube remains fairly constant.

As observed in the previous microstructure with no initial cube grain, the effect of introducing the extra $\{110\}\langle 110\rangle$ slip systems is not significant for a majority of the grains. While the presence of a cube oriented grain leads to some differences in the reorientation of individual elements of various grains, the deformations are by and large quite similar with and without the cube grain. However, a few of the grains, either due to their location or their orientation, show significant differences in deformation with 12 and 18 slip systems.

Finally, it is worthwhile to mention that for the deformation of the single crystal near cube, only at fairly large strains is there an appreciable difference in textures between 12 and 18 slip systems. However, for the case of a polycrystal, 50% reduction is enough to bring about significant differences between deformation with 12 and 18 slip systems. This is another indication of the effect of grain interactions, which lead to more heterogeneous deformation state compared to the boundary conditions of plane strain compression.

Conclusions

The deformations of single and polycrystals of aluminum have been simulated using the finite element method to study the effect of including slip on $\{110\}\langle 110\rangle$ systems. Simulations with initially near cube oriented single crystals show that slip on $\{110\}$ planes stabilizes the cube orientation, with the crystal rotating towards cube during plane strain compression. The same trend is also observed in a cube oriented crystal which is part of a polycrystalline aggregate.

The results presented here are in general agreement with experimental data on hot deformed aluminum alloys. In particular, slip on $\{110\}$ planes favoring stability of cube oriented grains has been observed in both single crystals and polycrystals. The simulations show the capability of the finite element approach to model the non-uniform deformations of both single crystals and different grains in the microstructure. These types of simulations can serve as valuable tools in providing better insights into the local variations in deformation and texture evolution within the individual grains of polycrystalline materials.

Acknowledgments

This research was sponsored by the Office of Basic Energy Sciences, U.S. Department of Energy, under contract DE-AC05-96OR22464 with Lockheed Martin Energy Research Corporation. The research was supported in part by an appointment to the Oak Ridge National Laboratory Postdoctoral Research Associates Program administered jointly by the Oak Ridge National Laboratory and the Oak Ridge Institute for Science and Education. The authors acknowledge the use of the Intel Paragon XP/S 35 located in the Oak Ridge National Laboratory Center for Computational Sciences (CCS), funded by the Department of Energy's Office of Scientific Computing.

References

1. Cl. Maurice and J.H. Driver, "Hot Rolling Textures of f.c.c. Metals—Part I. Experimental Results on Al Single and Polycrystals," Acta Mater., 45 (12) (1997), 4627–4638.

2. B. Bacroix and J.J. Jonas, "The Influence of Non-Octahedral Slip on Texture Development in FCC Metals," Textures and Microstructures, 8 & 9 (1988), 267–311.

3. R. Becker and S. Panchanadeeswaran, "Effects of Grain Interactions on Deformation and Local Texture in Polycrystals," Acta Mater., 43 (7) (1995), 2701–2719.

4. G.B. Sarma and P.R. Dawson, "Effects of Interactions among Crystals on the Inhomogeneous Deformations of Polycrystals," Acta Mater., 44 (5) (1996), 1937–1953.

5. A.J. Beaudoin, Jr., H. Mecking and U.F. Kocks, "Development of Localized Orientation Gradients in fcc Polycrystals," Phil. Mag. A, 73 (6) (1996), 1503–1517.

6. A. Akef and J.H. Driver, "Orientation Splitting of Cube-Oriented Face-Centered Cubic Crystals in Plane Strain Compression," Mater. Sci. Engng. A, 132 (1991), 245–255.

7. Cl. Maurice and J.H. Driver, "High Temperature Plane Strain Compression of Cube Oriented Aluminum Crystals," Acta Mater., 41 (6) (1993), 1653–1664.

8. A.J. Beaudoin et al., "A Hybrid Finite Element Formulation for Polycrystal Plasticity with Consideration of Macrostructural and Microstructural Linking," Int. J. Plasticity, 11 (1995), 501–521.

9. A.J. Beaudoin et al., "Application of Polycrystal Plasticity to Sheet Forming," Comput. Meth. Appl. Mech. Engng., 117 (1994), 49–70.

10. G. Sarma, T. Zacharia and D. Miles, "On Using High Performance Fortran for Parallel Programming," Comp. and Math. with Applic., (1998), to appear.

11. K.K. Mathur and P.R. Dawson, "On Modeling the Development of Crystallographic Texture in Bulk Forming Processes," Int. J. Plasticity, 5 (1989), 67–94.

12. U.F. Kocks, Proc. Eighth Inter. Conf. on Textures of Mater. (ICOTOM 8) (Warrendale, PA: The Metallurgical Society, 1988), 31–36.

13. J.S. Kallend et al., "Operational Texture Analysis," Mater. Sci. Engng. A, 132 (1991), 1–11.

14. R. Becker and S. Panchanadeeswaran, "Crystal Rotations Represented as Rodrigues Vectors," Textures and Microstructures, 10 (1989), 167–194.

15. J. Hirsch and K. Lücke, "Mechanism of Deformation and Development of Rolling Textures in Polycrystalline F.C.C. Metals—II. Simulation and Interpretation of Experiments on the Basis of Taylor-Type Theories," Acta Mater., 36 (11) (1988), 2883–2904.